hv photonics

IMPACT FACTOR 2.4

CITESCORE 2.3

Article

Enhanced Entanglement of the Two Cavity Modes in the Laguerre–Gaussian Cavity Optorotating System via an Optical Parametric Amplifier

Yupeng Chen, Sumei Huang, Li Deng and Aixi Chen

MDPI

https://doi.org/10.3390/photonics10080926

photonics

MDPI

Article

Enhanced Entanglement of the Two Cavity Modes in the Laguerre–Gaussian Cavity Optorotating System via an Optical Parametric Amplifier

Yupeng Chen [1], Sumei Huang [1], Li Deng [2] and Aixi Chen [1,*]

[1] Key Laboratory of Optical Field Manipulation of Zhejiang Province, Department of Physics, Zhejiang Sci-Tech University, Hangzhou 310018, China; 202220102053@mails.zstu.edu.cn (Y.C.); sumei@zstu.edu.cn (S.H.)
[2] School of Science, Zhejiang Sci-Tech University, Hangzhou 310018, China; lideng75@zstu.edu.cn
* Correspondence: aixichen@zstu.edu.cn

Abstract: Quantum entanglement in macroscopic systems plays an important role in quantum information processing. Here, we show that the steady-state entanglement between the two cavity modes in the macroscopic Laguerre–Gaussian (L–G) cavity optorotating system can be enhanced by placing a degenerate optical parametric amplifier (OPA) inside the cavity. The two L–G cavity modes are coupled to the same rotating mirror and are respectively driven at the red and blue mechanical sidebands. We use the logarithmic negativity to quantify the steady-state entanglement between the two cavity modes. We study the influences of the nonlinear gain and phase of the OPA, the temperature of the environment, and the angular momentums of the two cavity modes on the entanglement between the two cavity modes. In the cryogenic environment temperatures, when the angular momentums of the two cavity modes are identical, the enhancement of the entanglement between the two cavity modes by the OPA is the most significant.

Keywords: optomechanics; rotating mirror; enhanced entanglement; optical parametric amplifier

Citation: Chen, Y.; Huang, S.; Deng, L.; Chen, A. Enhanced Entanglement of the Two Cavity Modes in the Laguerre–Gaussian Cavity Optorotating System via an Optical Parametric Amplifier. *Photonics* **2023**, *10*, 926. https://doi.org/10.3390/photonics10080926

Received: 4 July 2023
Revised: 2 August 2023
Accepted: 8 August 2023
Published: 11 August 2023

1. Introduction

Quantum entanglement is the essence of quantum mechanics [1] and is widely used in a variety of quantum processes as an important resource, especially in quantum communication and quantum computation, so achieving the highly entangled quantum states is significant. Up to now, there have been many achievements in the study of quantum entanglement at the microscopic scale, while the progress is slow at the macroscopic scale.

Radiation pressure was first predicted by Johannes Kepler in 1619. Radiation pressure can lead to the interaction between a cavity field and a mechanical oscillator, which is the foundation of cavity optomechanics [2]. The optomechanical system is regarded as one of the best platforms to prepare entangled states, and the entanglement in the optomechanical system has been implemented between different modes, such as a cavity mode and a movable mirror [3–5], two cavity modes [6,7], two mechanical oscillators [8], even among an atom, a cavity mode, and a moving mirror [9].

In recent years, the Laguerre–Gaussian (L–G) cavity optorotating system has attracted a great deal of interest in quantum optics, in which the L–G beam interacts with the rotating mirror by the transfer of orbital angular momentum [10]. The rotating mirror is a spiral phase element [11] and can change the orbital angular momentum of the L–G beam via reflection or transmission [12]. Many phenomena have been observed in the L–G cavity optorotating system. The rotation mirror can release excitation quanta to implement the cooling of the rotational mirror by exchanging the orbital angular momentum with the L–G cavity mode [13]. A scheme to cool the rotation mirror in a Double L–G cavity optomechanical system was proposed with fewer strict limitations [14]. The L–G cavity optorotating

system can generate the L–G sum-sideband effect in matching conditions [15] and the second-order sideband effect [16]. Moreover, one can observe optomechanical-induced transparency (OMIT) [17] and Double-OMIT [18] in the L–G cavity optorotating systems, and the orbital angular momentum in the L–G cavity optorotating system can be detected via OMIT [17]. The L–G cavity optorotating system can also generate Fano resonance and realize slow-to-fast light conversion [19]. In addition, the L–G cavity optorotating system can be used to prepare the entanglement between various kinds of modes such as the cavity mode and a rotating mirror [10], among the cavity mode, a rotating mirror, and a magnon mode [20], and two rotating mirrors [21].

It is well known that an optical parametric amplifier (OPA) can be used to generate the squeezing of the cavity mode [22]. It has been reported that adding the OPA into an optomechanical cavity can produce many physical phenomena. The OPA can enhance the cooling of mechanical oscillators [23] and increase normal mode splitting [24]. It can also enhance single-photon weak coupling to strong coupling [25]. Furthermore, the OPA can enhance the entanglement between the two cavity modes [26], the entanglement between the cavity mode and a movable mirror [27,28], the entanglement between the two mechanical modes [29], and even the entanglement between the atom and the mirror [30].

In this paper, we study the enhancement of the entanglement between the two L–G cavity modes in the L–G cavity optorotating system with one rotating mirror via a degenerate OPA. The two cavity modes interact with the same rotating mirror. We choose the appropriate parameters to prepare the entangled state between the two cavity modes. The results indicate that the OPA can significantly enhance the stationary entanglement between the two cavity modes. In the steady state, we find that the enhancement of the entanglement is related to the nonlinear gain of the OPA, the phase of the optical driving of the OPA, the angular momentums of the cavity modes, and the temperature of the environment. The optimal nonlinear gain of the OPA to maximize the entanglement is influenced by the phase of the OPA and the temperature of the environment. For the higher nonlinear gain of the OPA, the entanglement between the two cavity modes is not larger. In addition, when the two cavity modes have identical angular momentums, the enhancement of the entanglement is the most significant, and the effect of the different angular momentums on the entanglement of the two cavity modes is similar to that of the large nonlinear gain on the entanglement of the two cavity modes.

The structure of this paper is as follows: in Section 2, we introduce the studied system and write the Hamiltonian. We then derive the quantum Langevin equations and give the mean values of the system operators. We use the Logarithmic negativity to quantify the entanglement between the two cavity modes. In Section 3, we show the results of the numerical calculations and we analyze the effects of the nonlinear gain and phase of the OPA, the temperature of the environment, and the angular momentums of the L–G cavity modes on the entanglement between the two cavity modes. In Section 4, we draw the conclusions.

2. Langevin Equations of the System

The system to be studied is shown in Figure 1, in which a degenerate OPA is placed in the L–G cavity optorotating system formed by two cavity modes and two cavity mirrors. The two cavity mirrors are the spiral phase elements [13]. The input mirror is fixed and the rear mirror is set on support S and can rotate about the Z axis. We use ϕ to represent the angle of its rotation. So we can treat the rear mirror as a harmonic oscillator with frequency ω_ϕ, which is described by the angle ϕ and the angular momentum L_z. The input mirror can reflect and transmit the light. It can remove the topological charge, $2l$, of the cavity mode in reflection and does not change the angular momentum in transmission. The rear mirror is considered as a completely reflecting mirror and can add the topological charge, $2l$, to the cavity mode. After a photon moves through a system one cycle, the torque exerted by the photons in the cavity on the rear mirror is given by $M = \frac{cl\hbar}{L}$, where c is the speed of light in vacuum and L is the length of the cavity [13].

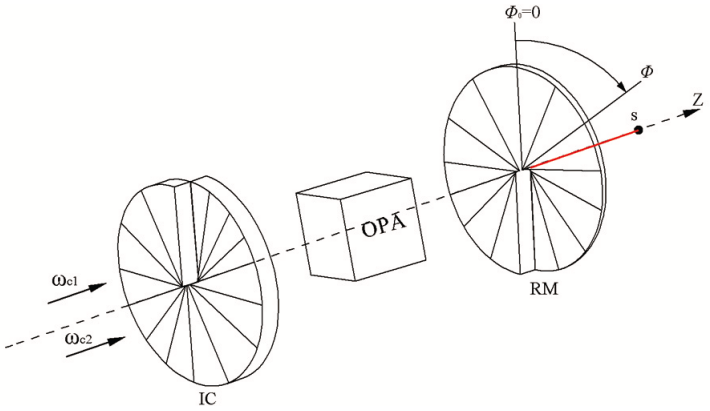

Figure 1. Sketch of the studied system. One red-detuned laser with frequency ω_{c1} and one blue-detuned laser with frequency ω_{c2} drive the two cavity modes in an optical cavity with two spiral phase elements (IC and RM) and a degenerate optical parametric amplifier (OPA). The RM is set on support S and can rotate about the Z axis. We use ϕ to represent the angle of its rotation. The two cavity modes interact simultaneously with the RM by the angular momentum exchange [13].

The two cavity modes with frequencies $\omega_{ci}(i = 1, 2)$ are driven by two Gaussian laser beams with frequencies $\omega_{Li}(i = 1, 2)$ and topological charge 0 through the left cavity mirror. For simplicity, the OPA is driven by two lasers with frequencies $2\omega_{Li}(i = 1, 2)$, and we assume that two frequencies, $\omega_{Li}(i = 1, 2)$, are very close so that $|\omega_{L1} - \omega_{L2}| << \Delta_c$, where $\Delta_c = \frac{\pi c}{L}$ is the free spectral range of the optical cavity, and c is the light speed in vacuum. When $L = 5$ mm, Δ_c is approximately 10^{11} Hz. Under this condition, the two cavity modes can interact with the OPA simultaneously, so the nonlinear processes can be written in the same form [26]. The two cavity modes, which are influenced by the OPA, interact simultaneously with the rear mirror by the angular momentum exchange. We can write the Hamiltonian of the whole system in the rotating frame at the frequencies of the input lasers as the following form:

$$\begin{aligned} H =& \frac{\hbar\omega_\phi}{2}(L_z^2 + \phi^2) + \sum_{i=1}^{2}\hbar(\omega_{ci} - \omega_{Li})a_i^\dagger a_i - \sum_{i=1}^{2}\hbar g_i a_i^\dagger a_i \phi \\ &+ \sum_{i=1}^{2} i\hbar G(e^{i\theta}a_i^{\dagger 2} - e^{-i\theta}a_i^2) + \sum_{i=1}^{2} i\hbar\varepsilon_i(a_i^\dagger - a_i), \end{aligned} \tag{1}$$

where a_i and $a_i^\dagger$ are the annihilation and creation operators of the cavity mode with frequency ω_{ci}. The first term is the energy of the rear mirror, where ϕ and L_z are the dimensionless angle and angular momentum operators (they obey the standard commutation relation $[\phi, L_z] = i$). The second term is the energies of the cavity modes. The third term describes the interactions of the cavity modes with the rear mirror, and $g_i = \frac{cl}{L}\sqrt{\frac{\hbar}{I\omega_\phi}}$ is the optomechanical coupling coefficient of a photon with frequency w_{ci}, where I is the moment of inertia of the rear mirror. The fourth term is the interactions of the cavity modes with the OPA, G is the nonlinear gain of the OPA, which is associated with the power of the driving field of the OPA, and θ is the phase of the optical field driving the OPA. Because the two cavity modes interact with the OPA simultaneously, G and θ are identical for the two cavity modes. The last term is the interactions of the cavity modes and the driving lasers, $\varepsilon_i = \sqrt{\frac{2\kappa P_i}{\hbar\omega_{Li}}}$ is the coupling between the driving laser and the cavity mode, where $\kappa = \frac{\pi c}{2FL}$ is the decay rate of the cavity with the cavity finesse, F, and P_i is the power of the driving laser. It has been shown that the effect of the degenerate OPA on the optomechnical entanglement is equivalent to that of a periodically modulated external field [5,28].

The Langevin equations of the system can be derived from the Heisenberg equation of motion. Considering the Brownian noise, the vacuum noise, and the damping of the system, we can write Langevin equations in the interaction picture:

$$\begin{aligned}
&\dot{\phi} = \omega_\phi L_z, \\
&\dot{L_z} = -\omega_\phi \phi + g_1 a_1^\dagger a_1 + g_2 a_2^\dagger a_2 - \frac{D_\phi}{I} L_z + \xi, \\
&\dot{a_i} = -(\kappa + i\Delta_{0i}) a_i + i g_i a_i \phi + \varepsilon_i + 2Ge^{i\theta} a_i^\dagger + \sqrt{2\kappa} a_{i_{in}},
\end{aligned} \tag{2}$$

where $\Delta_{0i} = \omega_{ci} - \omega_{Li}$ is the cavity detuning, D_ϕ is the intrinsic damping constant of the rotating mirror, and $i = 1, 2$. $a_{i_{in}}$ is the operator of the input vacuum noise of the cavity mode, whose only nonzero correlation function is [22]

$$\langle a_{i_{in}}(t) a_{i_{in}}^\dagger(t) \rangle = \delta(t - t'). \tag{3}$$

ξ is the Hermitian Brownian noise operator, whose correlation function is [31,32]

$$\langle \xi(t) \xi(t') \rangle = \frac{D_\phi}{\omega_\phi I} \int \frac{d\omega}{2\pi} e^{-i\omega(t-t')} \omega [1 + coth(\frac{\hbar\omega}{2k_B T})], \tag{4}$$

where k_B is the Boltzmann's constant and T is the temperature of the environment.

We then calculate the expectation values of the system operators in the steady state. We use the expectation values of the system operators to rewrite Equation (2). Because the system is in the steady state, their expectation values do not change with time. We can obtain $\langle a_i^\dagger a_i \rangle = \langle a_i^\dagger \rangle \langle a_i \rangle$ and $\langle a_i \phi \rangle = \langle a_i \rangle \langle \phi \rangle$ due to the large amplitudes of the cavity modes. The mean values of the system operators in the steady state are given by:

$$\begin{aligned}
&L_{zs} = 0, \\
&\phi_s = \frac{g_1 |a_{1s}|^2 + g_2 |a_{2s}|^2}{\omega_\phi}, \\
&a_{is} = \frac{\varepsilon_i}{(\kappa - 2Gcos\theta) + i(\Delta_i - 2Gsin\theta)},
\end{aligned} \tag{5}$$

where subscript s represents the steady-state value of operators, $\Delta_i = \Delta_{0i} - g_i \phi_s$ is the effective cavity detuning, and $i = 1, 2$. At the steady state, the angular momentum, L_{zs}, of the rotating mirror is zero, and the angle, ϕ_s, of the rotating mirror depends on the steady-state amplitudes, a_{is}, of the two cavity modes. We can see that the OPA changes the decay rate, κ, to $\kappa - 2Gsin\theta$ and the effective cavity detuning, Δ_i, to $\Delta_i - 2Gsin\theta$, and a_{is} depends on the OPA. By choosing the appropriate parameters of the system, a_{is} can be a real number ($a_{is} = a_{is}^*$). We use two high-power lasers to drive the two cavity modes, so we can rewrite each operator as the steady-state mean value plus a fluctuation operator, $\phi = \phi_s + \delta\phi$, $L_z = L_{zs} + \delta L_z$, $a_i = a_{is} + \delta a_i$, and insert them into the Langevin equations of Equation (2); we obtain the quantum Langevin equations:

$$\begin{aligned}
&\dot{\delta\phi} = \omega_\phi \delta L_z, \\
&\delta\dot{L}_z = -\omega_\phi \delta\phi + g_1 a_{1s} (\delta a_1^\dagger + \delta a_1) + g_2 a_{2s} (\delta a_2^\dagger + \delta a_2) - \frac{D_\phi}{I} \delta L_z + \xi, \\
&\dot{\delta a_i} = -(\kappa + i\Delta_i) \delta a_i + i g_i a_{is} \delta\phi + 2Ge^{i\theta} \delta a_i^\dagger + \sqrt{2\kappa} a_{i_{in}} (i = 1, 2),
\end{aligned} \tag{6}$$

where we have ignored small quantities of higher order and $i = 1, 2$. We define the amplitude fluctuation operators and the phase fluctuation operators of the cavity modes as $\delta X_i = \frac{1}{\sqrt{2}}(\delta a_i + \delta a_i^\dagger)$, $\delta Y_i = \frac{1}{\sqrt{2}i}(\delta a_i - \delta a_i^\dagger)$ and the quadrature operators of the vacuum noise as $X_{i_{in}} = \frac{1}{\sqrt{2}}(a_{i_{in}} + a_{i_{in}}^\dagger)$ and $Y_{i_{in}} = \frac{1}{\sqrt{2}i}(a_{i_{in}} - a_{i_{in}}^\dagger)$. Finally, the linearized Langevin equations are given as:

$$\begin{aligned}
\delta\dot{\phi} &= \omega_\phi \delta L_z, \\
\delta\dot{L}_z &= -\omega_\phi \delta\phi + G_1 \delta X_1 + G_2 \delta X_2 - \frac{D_\phi}{I}\delta L_z + \xi, \\
\delta\dot{X}_i &= -(\kappa - 2Gcos\theta)\delta X_i + (\Delta_i + 2Gsin\theta)\delta Y_i + \sqrt{2\kappa}X_{i_{in}}, \\
\delta\dot{Y}_i &= -(\kappa + 2Gcos\theta)\delta Y_i - (\Delta_i - 2Gsin\theta)\delta X_i + G_i\delta\phi + \sqrt{2\kappa}Y_{i_{in}},
\end{aligned} \tag{7}$$

where $G_i = \sqrt{2}g_i a_{is}$ is the effective optomechanical coupling strength and can be adjusted by changing the powers of the input lasers, $i = 1, 2$. We can rewrite Equation (7) in the following form:

$$\dot{u}(t) = Au(t) + n(t), \tag{8}$$

where $u(t) = (\delta\phi, \delta L_z, \delta X_1, \delta Y_1, \delta X_2, \delta Y_2)^\top$ is the vector of fluctuation operators, $n(t) = (0, \xi(t), \sqrt{2\kappa}X_{1_{in}}(t), \sqrt{2\kappa}Y_{1_{in}}(t), \sqrt{2\kappa}X_{2_{in}}(t), \sqrt{2\kappa}Y_{2_{in}}(t))^\top$ is the vector of noises, and A is a 6×6 matrix:

$$A = \begin{pmatrix}
0 & \omega_\phi & 0 & 0 & 0 & 0 \\
-\omega_\phi & -\frac{D_\phi}{I} & G_1 & 0 & G_2 & 0 \\
0 & 0 & -\kappa + 2Gcos\theta & \Delta_1 + 2Gsin\theta & 0 & 0 \\
G_1 & 0 & -\Delta_1 + 2Gsin\theta & -\kappa - 2Gcos\theta & 0 & 0 \\
0 & 0 & 0 & 0 & -\kappa + 2Gcos\theta & \Delta_2 + 2Gsin\theta \\
G_2 & 0 & 0 & 0 & -\Delta_2 + 2Gsin\theta & -\kappa - 2Gcos\theta
\end{pmatrix}. \tag{9}$$

The system is stable only when all of the eigenvalues of matrix A have negative real parts. We can obtain the stable conditions by the Routh–Hurwitz criterion [33], but the process of the calculation is too complex and we will not write it in this paper. The quantum noises of the system are in a Gaussian state, and the quantum Langevin equations are linearized, thus the system is always in a three-mode Gaussian state with two cavity modes and one mechanical mode, which can be described by the 6×6 convariance matrix V, with its elements defined by $V_{ij} = (\langle u_i(\infty)u_j(\infty) + u_j(\infty)u_i(\infty)\rangle)/2$. In the system we observe the entanglement of the two cavity modes in the steady state, which can be calculated by covariance matrix V of the system. Covariance matrix V of the system can be obtained via solving the Lyapunov equation:

$$AV + VA^\top = -D, \tag{10}$$

where the elements of matrix D are given as $\frac{1}{2}\langle n_i(t)n_j(s) + n_j(s)n_i(t)\rangle = D_{ij}\delta(t-s)$. Currently, the quality factor, $Q = \frac{\omega_\phi}{D_\phi/I} \gg 1$, of the rotating mirror can be achieved in the experiment [8]. In this limit, the correlation of ξ is given by [34]:

$$\frac{1}{2}\langle\xi(t)\xi(t') + \xi(t')\xi(t)\rangle \simeq \frac{D_\phi}{I}(2\bar{n}+1)\delta(t-t'), \tag{11}$$

where $\bar{n} = (e^{\frac{\hbar\omega_{eff}}{k_B T}} - 1)^{-1}$ is the mean number of thermal phonons of the rotating mirror and ω_{eff} is the effective frequency of the rotating mirror. We can then write matrix D as $D = diag[0, \frac{D_\phi}{I}(2\bar{n}+1), \kappa, \kappa, \kappa, \kappa]$, which is a diagonal matrix and obtained via Equations (11) and (3). After we insert matrices A and D into Equation (10) to obtain matrix V, the entanglement, E_N, of the two cavity modes can be quantified by the logarithmic negativity, which is defined as [35,36]:

$$E_N = max[0, -ln2\eta^-], \tag{12}$$

where $\eta^- \equiv 2^{-\frac{1}{2}}\{\sum(V') - [\sum(V')^2 - 4detV']^{\frac{1}{2}}\}^{\frac{1}{2}}$ with the 4×4 matrix V' and V' consists of the elements of V associated with the two cavity modes and *det* is the determinant of the matrix. We can rewrite matrix V' in the form of a 2×2 block:

$$V' = \begin{pmatrix} A & C \\ C^{\top} & B \end{pmatrix}, \tag{13}$$

to calculate $\sum(V') \equiv detA + detB - 2detC$. Here, A and B represent the variances of cavity mode 1 and cavity mode 2, respectively, while C describes the correlation between the two cavity modes.

3. Numerical Calculation of E_N and Discussion

In this section, we numerically investigate the influence of the OPA on the steady-state entanglement between the two cavity modes. In order to observe the influence of the OPA obviously, we need to choose the appropriate effective cavity detunings to generate the large entanglement. Similar to [26], we set the effective detunings of the two cavity modes in the red and blue mechanical sidebands ($\Delta_1 = \omega_\phi$ and $\Delta_2 = -\omega_\phi$) to generate entanglement efficiently. The other parameters are given as follows [3,8,37]: the length of the cavity, L = 5 mm, the finesse of the cavity, $F = 10^5$, the mass of the rotating mirrors, $m = 5$ ng, the radius of the rotating mirrors, R = 10 μm, the resonance frequency of the rotating mirror, $\omega_\phi = 2\pi \times 10$ MHz, the effective frequency of the rotating mirror, $\omega_{eff} = 0.8\omega_\phi$, the quality factor of the rotating mirror, $Q = 10^7$, the powers of two driven lasers, $P_1 = 100$ mW, $P_2 = 95$ mW, and the wavelengths of the two input lasers, $\lambda = 1064$ nm. Under these conditions, we can obtain $\kappa = 3\pi \times 10^5$ and $\frac{D_\phi}{I} = 2\pi$. Thus, our system is working in the resolved sideband limit, $\omega_\phi >> \kappa >> \frac{D_\phi}{I}$. When cavity mode 2 is driven by a blue-detuned laser, $\Delta_2 = -\omega_\phi$, the entanglement between cavity mode 2 and the rotating mirror is created. When cavity mode 1 is driven by a red-detuned laser, $\Delta_1 = \omega_\phi$, the quantum state of the rotating mirror is transferred to cavity mode 1. Undergoing these two processes, quantum entanglement is created between the two cavity modes. Moreover, an L–G laser beam with a topological charge value up to $l = 1000$ can be generated by using spiral phase elements experimentally [11].

Figure 2 shows the entanglement, E_N, of the two cavity modes as a function of phase θ of the OPA in the range of $\theta \in [0, \pi]$. By numerical simulations, we find that the system is stable in the range of phases $\theta \in [0, \pi]$, while the system is unstable in the range of phases $\theta \in [\pi, 2\pi]$. Without the OPA ($G = 0$), when the phase of the OPA is changed from 0 to π, E_N remains unchanged ($E_N = 0.264$). With the OPA ($G \neq 0$), E_N is larger than 0.264 when θ is larger than 0 but less than π, which indicates that the OPA can enhance the entanglement between the two cavity modes by squeezing the optical field [38]. Meanwhile, we find there is an optimal phase, θ, to achieve the maximum entanglement in a lower gain, G, which is $\theta = \frac{\pi}{2}$. With the gain increasing, the optimal phase moves toward 0 and π.

Figure 3 shows the entanglement, E_N, of the two cavity modes as a function of the nonlinear gain, G, of the OPA for the various phases, θ, of the OPA. When $\theta = 0$, the entanglement between the two cavity modes decreases by increasing the parametric gain, G, of the OPA. When θ is nonzero, by increasing the parametric gain, G, of the OPA, the entanglement between the two cavity modes first increases then decreases. For a larger parametric phase, θ, the maximum entanglement becomes larger and happens at a lower parametric gain, G, of the OPA. Figure 4 shows the effect of the nonlinear gain, G, of the OPA on the entanglement between the two cavity modes for different temperatures, T, of the environment. Compared to the entanglement without the OPA ($G = 0$), it is seen that the maximum entanglement is significantly enhanced by the OPA, which increases by 114% for $T = 10$ mK, increases by 89% for $T = 50$ K, increases by 75% for $T = 100$ K, and increases by 66% for $T = 150$ K. Thus, the enhancement of the entanglement by the OPA is the most significant for the lowest temperature, $T = 10$ mK. We also see that the maximum entanglement decreases with the increase in temperature, T, of the environment.

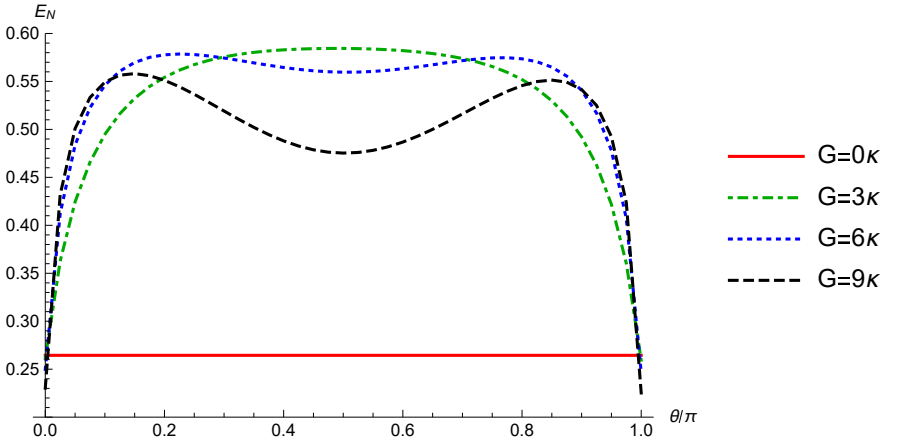

Figure 2. The entanglement, E_N, of the two cavity modes as a function of the phase, θ, of the OPA for various nonlinear gains, G, of the OPA. The solid, dot-dashed, dotted, and dashed curves represent $G = 0, 3\kappa, 6\kappa, 9\kappa$, respectively. The other parameters are $l_1 = l_2 = 100\hbar$, $T = 10$ mK.

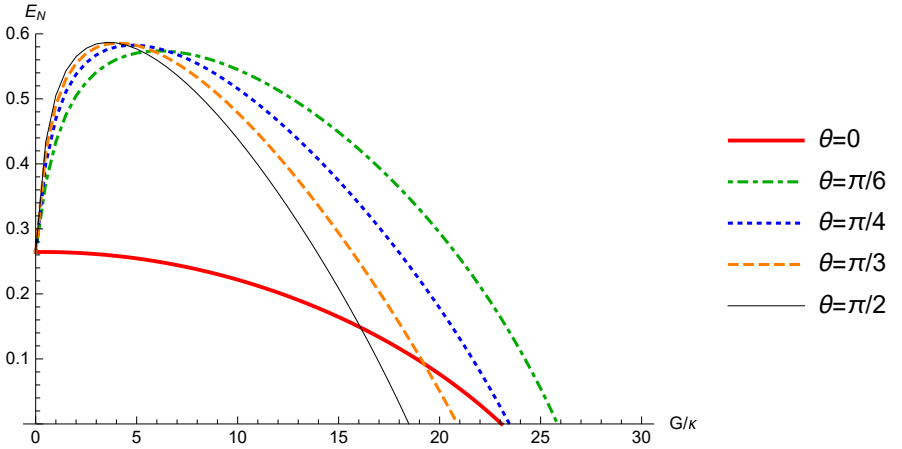

Figure 3. The entanglement, E_N, of the two cavity modes as a function of the nonlinear gain, G, of the OPA for the various phases, θ, of the OPA. The thick-solid, dot-dashed, dotted, dashed, and thin-solid curves represent $\theta = 0, \pi/6, \pi/4, \pi/3, \pi/2$, respectively. The other parameters are $l_1 = l_2 = 100\hbar$, $T = 10$ mK.

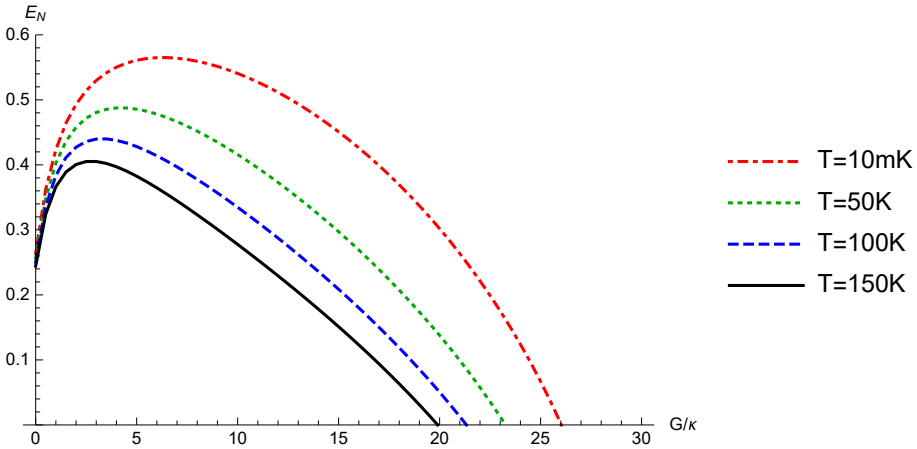

Figure 4. The entanglement, E_N, of the two cavity modes as a function of the nonlinear gain, G, for various system temperatures, T. The dot-dashed, dotted, dashed, and solid curves represent T = 10 mK, 50 K, 100 K, 150 K, respectively. The other parameters are $l_1 = l_2 = 100\hbar$, $\theta = 0.85\pi$.

From Figures 3 and 4, it is noted that the bigger nonlinear gain, G, of the OPA does not lead to the larger entanglement between the two cavity modes. Thus, there exists

an optimal nonlinear gain, G, to achieve the maximum entanglement. Figure 5 plots the optimal nonlinear gain, G, for achieving the maximum entanglement as a function of the temperature, T, of the environment, where $l_1 = l_2 = 100\hbar$, $\theta = 0.85\pi$. It is seen that the optimal nonlinear gain, G, decreases with the increase in temperature, T, of the environment. For example, when $T = 10$ mK, 50 K, 100 K, 150 K, 200 K, 250 K, the optimal nonlinear gain, G, is 6.5κ, 4.2κ, 3.3κ, 2.8κ, 2.4κ, 2.1κ, respectively. It is seen that the entanglement can exist even at $T = 250K$; thus, the entanglement is robust against the temperature of the environment in the presence of the OPA.

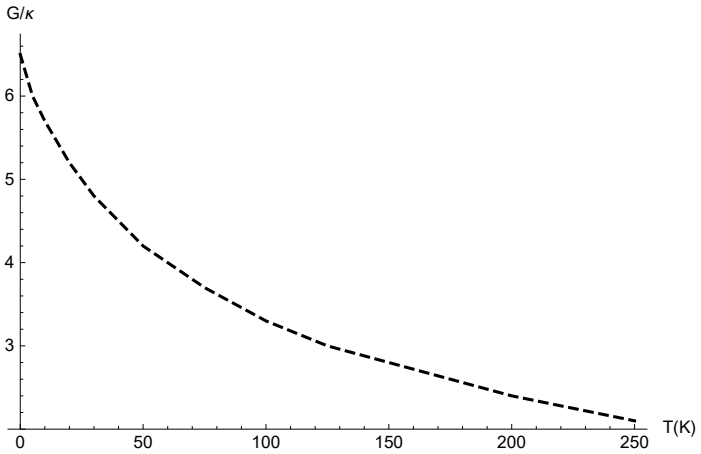

Figure 5. The optimal nonlinear gain, G, for the entanglement as a function of the temperature, T, of the environment. The other parameters are $l_1 = l_2 = 100\hbar$, $\theta = 0.85\pi$.

The explanation of reducing the entanglement for a larger nonlinear gain are as follows. On the one hand, the effective detuning of the two cavity modes are different ($\Delta_{1,2} = \pm\omega_\phi$). With the increase in the nonlinear gain, G, photon number $|a_{1s}|^2$ increases, while photon number $|a_{2s}|^2$ decreases, as shown in Figure 6, which makes the difference between G_1 and G_2 larger for a larger nonlinear gain. This can also explain the phenomenon in Figure 3, when $\theta = \frac{\pi}{2}$, the increasing of the difference between $|a_{1s}|^2$ and $|a_{2s}|^2$ is the fastest, so the entanglement can reach the maximum value for the lowest nonlinear gain, G, and then reduce. On the other hand, the squeezings of the two cavity modes are different for a larger nonlinear gain, and the difference between the squeezing degrees of the two cavity modes is larger with the growing of the nonlinear gain [26], as shown in Figure 7. Figure 7 shows the degree of squeezing of the two cavity modes as a function of the nonlinear gain, G, of the OPA. In this figure, we use the ratio $\langle \delta X_1^2 \rangle / \langle \delta Y_1^2 \rangle$ to represent the degree of squeezing of cavity mode 1 and the ratio $\langle \delta Y_2^2 \rangle / \langle \delta X_2^2 \rangle$ to represent the degree of squeezing of cavity mode 2. Without OPA ($G = 0$), $\langle \delta X_1^2 \rangle / \langle \delta Y_1^2 \rangle$ and $\langle \delta Y_2^2 \rangle / \langle \delta X_2^2 \rangle$ are equal to 1; thus, the two cavity modes 1 and 2 are not squeezed, because without OPA the cavity modes are in the thermal states [26] due to their interactions with the rotating mirror in thermal equilibrium with its surrounding environment. With the increase in the nonlinear gain, G, $\langle \delta X_1^2 \rangle / \langle \delta Y_1^2 \rangle$ and $\langle \delta Y_2^2 \rangle / \langle \delta X_2^2 \rangle$ increase, which shows that the OPA squeezes the phase quadrature of cavity mode 1 and the amplitude quadrature of cavity mode 2, and the degrees of squeezing for the two cavity modes are very close for a lower nonlinear gain, G, while the difference of squeezing degrees between the two cavity modes is more obvious for a higher nonlinear gain, G. For a lower nonlinear gain G, the squeezings of the two cavity modes increase the entanglement of the two cavity modes, but for a higher nonlinear gain G, the squeezings of the two cavity modes decrease the entanglement of the two cavity modes. Therefore, for a larger nonlinear gain, G, the optical noise becomes an important effective thermal bath coupled to the mechanical oscillator, giving rise to the decrease in the entanglement between the two cavity modes [26].

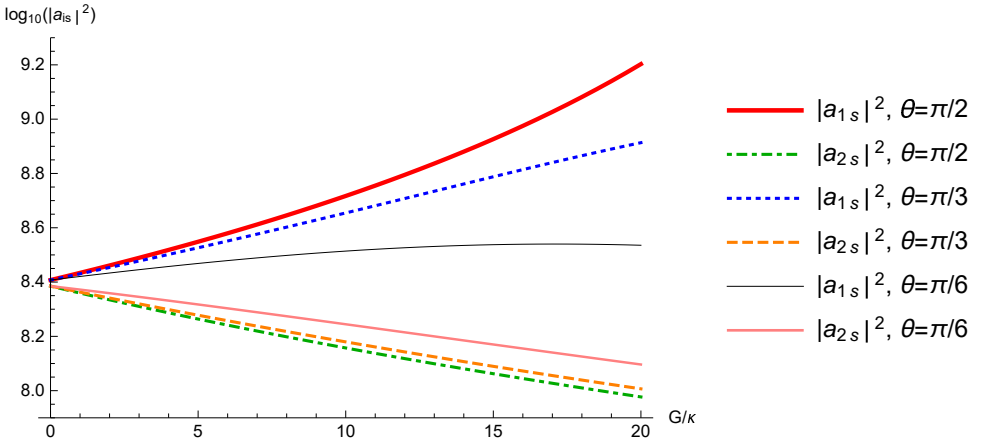

Figure 6. The Logarithmic number of photons, $|a_{is}|^2$, as a function of the nonlinear gain, G, for the various phases, θ, of the OPA. The thick-solid, dot-dashed, dotted, dashed, thin-solid, and solid curves represent $|a_{1s}|^2$ when $\theta = \pi/2$, $|a_{2s}|^2$ when $\theta = \pi/2$, $|a_{1s}|^2$ when $\theta = \pi/3$, $|a_{2s}|^2$ when $\theta = \pi/3$, $|a_{1s}|^2$ when $\theta = \pi/6$, and $|a_{2s}|^2$ when $\theta = \pi/6$, respectively. The other parameters are $l_1 = l_2 = 100\hbar$, $T = 10$ mK.

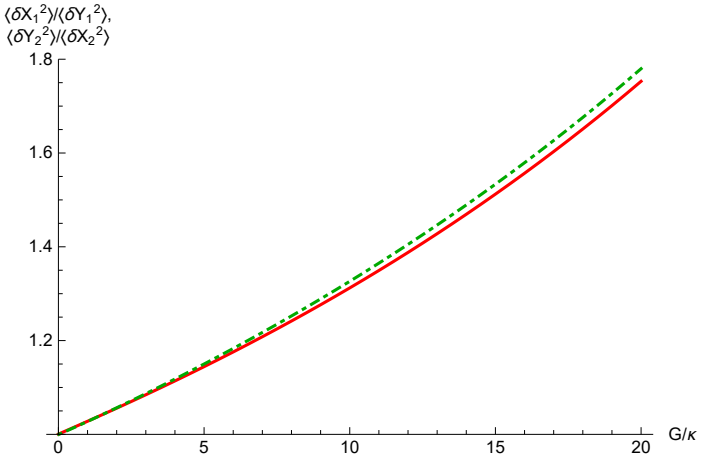

Figure 7. The degrees of squeezing of the two cavity modes as a function of the nonlinear gain, G, of the OPA. The solid and dot-dashed curves represent $\langle \delta X_1^2 \rangle / \langle \delta Y_1^2 \rangle$ and $\langle \delta Y_2^2 \rangle / \langle \delta X_2^2 \rangle$, respectively. The other parameters are $l_1 = l_2 = 100\hbar$, $T = 10$ mK, $\theta = 0.85\pi$.

Figure 8 shows the entanglement, E_N, of the two cavity modes as a function of the nonlinear gain, G, for various angular momentums of the two cavity modes. When $G = 0$, for $l_2 = 100\hbar$, $95\hbar$, $90\hbar$, $85\hbar$, $E_N = 0.264$, 0.439, 0.508, 0.542. The maximum values of E_N for $l_2 = 100\hbar$, $95\hbar$, $90\hbar$, $85\hbar$ are 0.565, 0.569, 0.569, 0.569. This shows that the enhancement of entanglement by the OPA is the largest when the angular momentums of the two cavity modes are the same and reduces with the increasing of the difference between the two angular momentums of the two cavity modes. The difference of the angular momentums of the two cavity modes has no distinct effect on the maximum entanglement.

Figure 9 shows the entanglement, E_N, of the two cavity modes as a function of the parametric phase, θ, of the OPA for various angular momentums of the two cavity modes. It shows that the effect of the parametric phase, θ, of the OPA on the entanglement, E_N, of the two cavity modes is smaller for the larger difference between the angular momentums of the two cavity modes. For $G = 6\kappa$, with increasing the difference between the two angular momentums, the optimal phase, θ, is shifted to $\theta = 0, \pi$. When $\theta = \frac{\pi}{2}$, the entanglement becomes weaker with the increasing of the difference between two angular momentums. Comparing Figure 9 with Figure 2, it can be seen that the effect of the different angular momentums on the entanglement of the two cavity modes is similar to that of the large nonlinear gain on the entanglement of the two cavity modes. The numerical calculations

show that the angular momentum only influences the optomechanical coupling coefficient, g_i, so that the effective optomechanical coupling strength, G_i, is changed. The effective optomechanical coupling strength, G_i, is plotted as a function of the nonlinear gain, G, for the different angular momentums of the two cavity modes, as shown in Figure 10. From Figure 10, it can be seen that G_1 increases with the increase in the nonlinear gain, G, while G_2 decreases with the increase in the nonlinear gain, G. When $G = 6\kappa$, the difference between G_1 and G_2 increases with a decrease in the angular momentum, l_2, leading to the weaker entanglement between the two cavity modes shown in Figure 9.

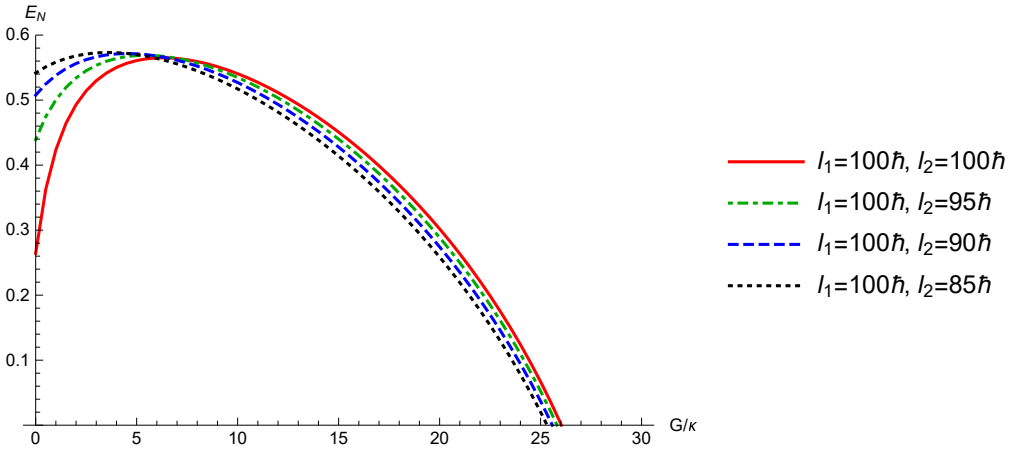

Figure 8. The entanglement, E_N, of the two cavity modes as a function of the nonlinear gain, G, for various angular momentums of the two cavity modes. The solid, dot-dashed, dashed, and dotted curves represent $l_2 = 100\hbar$, $95\hbar$, $90\hbar$, $85\hbar$, respectively. The other parameters are $l_1 = 100\hbar$, $T = 10$ mK, $\theta = 0.85\pi$.

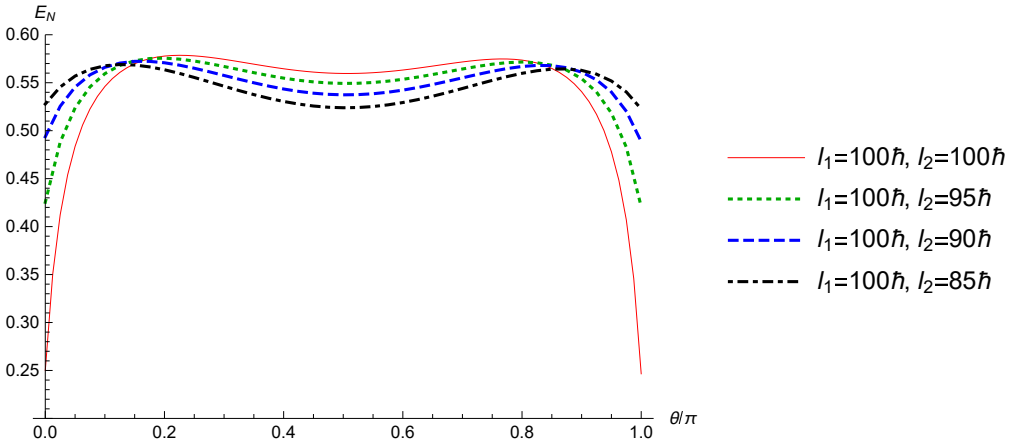

Figure 9. The entanglement, E_N, of the two cavity modes as a function of the parametric phase, θ, of the OPA for various angular momentums of the two cavity modes. The thin-solid, dotted, dashed, and dot-dashed curves represent $l_2 = 100\hbar$, $95\hbar$, $90\hbar$, $85\hbar$, respectively. The other parameters are $l_1 = 100\hbar$, $T = 10$ mK, $G = 6\kappa$.

Through the comparisons of the logarithmic negativity, E_N, of the two cavity modes in the presence of the OPA in the L–G cavity optorotating system and that in the optomechanical system, we find that the L–G cavity optorotating system has some advantages over the optomechanical system. The obvious advantage of the L–G cavity optorotating system is that the entanglement between the two cavity modes in the presence of the OPA is more robust against the temperature of the environment. The entanglement in the L–G cavity optorotating system with the OPA at $T = 100$ K is stronger than that in the optomechanical system with the OPA at $T = 0.1$ K [26], which means that we can implement the same entanglement of the two cavity modes in the L–G cavity optorotating system with the OPA

at a higher temperature of the environment. Thus, the L–G cavity optorotating system with the OPA releases the limitation of the cryogenic temperature to achieve the entanglement. We also observe that the maximum optimal nonlinear gain, G, in the L–G cavity optorotating system with the OPA is approximately 6κ, similar to that in the optomechanical system with the OPA. In addition, in the optomechanical system with the OPA [26], for different nonzero parametric gains, G, the maximum entanglement always happens at $\theta = \pi/2$. However, in the L–G optorotating system with the OPA, for different nonzero parametric gains, G, the maximum entanglement does not always happen at $\theta = \pi/2$. For $G = 3\kappa$, the maximum entanglement happens at $\theta = \pi/2$. With further increasing the parametric gain G, the maximum entanglement moves away from $\theta = \pi/2$ toward $\theta = 0$ and π, as shown in Figure 3, and the entanglement at $\theta = \pi/2$ decreases. Furthermore, the maximum entanglement between the two cavity modes and the enhancement of the entanglement between the two cavity modes induced by the OPA are also improved in the L–G cavity optorotating system.

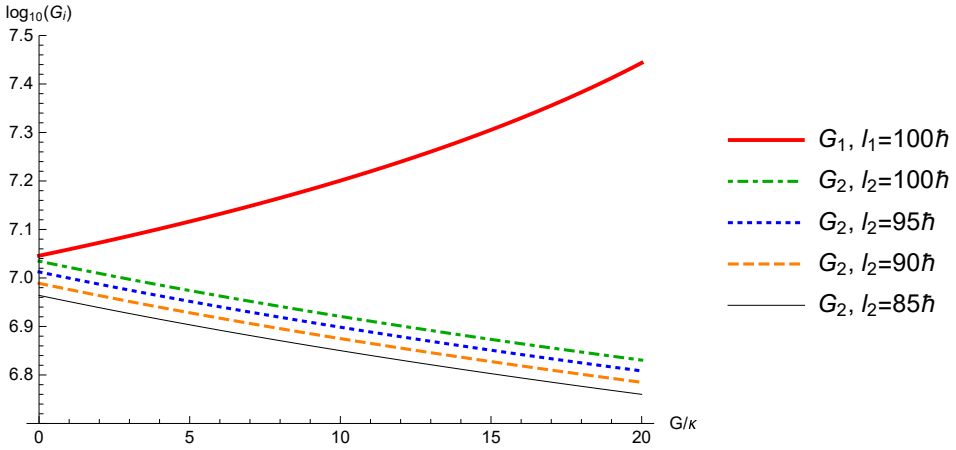

Figure 10. The Logarithmic effective optomechanical coupling strength, G_i, as a function of the nonlinear gain G. The thick-solid, dot-dashed, dotted, dashed, and thin-solid curves represent G_1 when $l_1 = 100\hbar$, G_2 when $l_2 = 100\hbar$, G_2 when $l_2 = 95\hbar$, G_2 when $l_2 = 90\hbar$, G_2 when $l_2 = 85\hbar$, respectively. The other parameters are $\theta = 0.5\pi$, $T = 10$ mK.

4. Conclusions

We have studied the effect of degenerate OPA on the steady-state entanglement of two L–G cavity modes, which interact with the same rotating mirror. We find that the OPA can significantly enhance the entanglement of the two cavity modes due to the squeezing of the two cavity modes induced by the OPA. The enhancement of the entanglement induced by the OPA is the most significant when the system is working in cryogenic environment temperatures and the two cavity modes have the same angular momentums. We find that the optimal nonlinear gain of the OPA to achieve the maximum entanglement depends on the parametric phase of the OPA and the temperature of the environment. Moreover, the entanglement of the two cavity modes can be further improved by using measurement-based feedback control [39] and coherent feedback control [40]. The generated entanglement of the two cavity modes in the macroscopic L–G cavity optorotating system with the OPA is a useful resource in the construction of quantum communication networks.

Author Contributions: Conceptualization, S.H. and A.C.; methodology, S.H. and A.C.; software, Y.C., S.H., and L.D.; formal analysis, Y.C., S.H., and L.D.; writing—original draft preparation, Y.C., S.H., and L.D.; writing—review and editing, S.H. and A.C. All authors have read and agreed to the published version of the manuscript.

Funding: This research was funded by the National Natural Science Foundation of China (grant numbers 12174344, 12175199, 91636108), by the Zhejiang Provincial Natural Science Foundation of

China (grant numbers LY21A040007, LZ20A040002), and by the Science Foundation of Zhejiang Sci-Tech University (grant numbers 18062121-Y, 17062071-Y).

Institutional Review Board Statement: Not applicable.

Informed Consent Statement: Not applicable.

Data Availability Statement: Not applicable.

Conflicts of Interest: The authors declare no conflict of interest.

References

1. Horodecki, R.; Horodecki, P.; Horodecki, M.; Horodecki, K. Quantum entanglement. *Rev. Mod. Phys.* **2009**, *81*, 865.
2. Aspelmeyer, M.; Kippenberg, T.J.; Marquardt, F. Cavity optomechanics. *Rev. Mod. Phys.* **2014**, *86*, 1391. [CrossRef]
3. Vitali, D.; Gigan, S.; Ferreira, A.; Böhm, H.; Tombesi, P.; Guerreiro, A.; Vedral, V.; Zeilinger, A.; Aspelmeyer, M. Optomechanical entanglement between a movable mirror and a cavity field. *Phys. Rev. Lett.* **2007**, *98*, 030405. [CrossRef]
4. Kleckner, D.; Marshall, W.; de Dood, M.J.; Dinyari, K.N.; Pors, B.J.; Irvine, W.T.; Bouwmeester, D. High finesse opto-mechanical cavity with a movable thirty-micron-size mirror. *Phys. Rev. Lett.* **2006**, *96*, 173901. [CrossRef] [PubMed]
5. Lin, W.; Liao, C.G. Enhancement of asymmetric steering via interference effects induced by twofold modulations in a cavity optomechanical system. *Eur. Phys. J. Plus* **2021**, *136*, 324. [CrossRef]
6. Tian, L. Robust photon entanglement via quantum interference in optomechanical interfaces. *Phys. Rev. Lett.* **2013**, *110*, 233602. [CrossRef]
7. Wang, Y.D.; Clerk, A.A. Reservoir-engineered entanglement in optomechanical systems. *Phys. Rev. Lett.* **2013**, *110*, 253601. [CrossRef]
8. Hartmann, M.J.; Plenio, M.B. Steady state entanglement in the mechanical vibrations of two dielectric membranes. *Phys. Rev. Lett.* **2008**, *101*, 200503. [CrossRef]
9. Genes, C.; Vitali, D.; Tombesi, P. Emergence of atom-light-mirror entanglement inside an optical cavity. *Phys. Rev. A* **2008**, *77*, 050307. [CrossRef]
10. Bhattacharya, M.; Giscard, P.L.; Meystre, P. Entanglement of a Laguerre-Gaussian cavity mode with a rotating mirror. *Phys. Rev. A* **2008**, *77*, 013827. [CrossRef]
11. Shen, Y.; Campbell, G.T.; Hage, B.; Zou, H.; Buchler, B.C.; Lam, P.K. Generation and interferometric analysis of high charge optical vortices. *J. Opt.* **2013**, *15*, 044005. [CrossRef]
12. Oemrawsingh, S.; Eliel, E.; Woerdman, J.; Verstegen, E.; Kloosterboer, J. Half-integral spiral phase plates for optical wavelengths. *J. Opt. A Pure Appl. Opt.* **2004**, *6*, S288. [CrossRef]
13. Bhattacharya, M.; Meystre, P. Using a Laguerre-Gaussian beam to trap and cool the rotational motion of a mirror. *Phys. Rev. Lett.* **2007**, *99*, 153603. [CrossRef]
14. Liu, Y.M.; Bai, C.H.; Wang, D.Y.; Wang, T.; Zheng, M.H.; Wang, H.F.; Zhu, A.D.; Zhang, S. Ground-state cooling of rotating mirror in double-laguerre-gaussian-cavity with atomic ensemble. *Opt. Express* **2018**, *26*, 6143–6157. [CrossRef] [PubMed]
15. Xiong, H.; Huang, Y.M.; Wu, Y. Laguerre-Gaussian optical sum-sideband generation via orbital angular momentum exchange. *Phys. Rev. A* **2021**, *103*, 043506. [CrossRef]
16. Kazemi, S.H.; Mahmoudi, M. Optomechanical second-order sideband effects in a Laguerre–Gaussian rotational-cavity system. *Phys. Scr.* **2020**, *95*, 045107. [CrossRef]
17. Peng, J.X.; Chen, Z.; Yuan, Q.Z.; Feng, X.L. Optomechanically induced transparency in a Laguerre-Gaussian rotational-cavity system and its application to the detection of orbital angular momentum of light fields. *Phys. Rev. A* **2019**, *99*, 043817. [CrossRef]
18. Peng, J.X.; Chen, Z.; Yuan, Q.Z.; Feng, X.L. Double optomechanically induced transparency in a Laguerre-Gaussian rovibrational cavity. *Phys. Lett. A* **2020**, *384*, 126153. [CrossRef]
19. Xu, Y.; Liu, W. Fano resonance and slow-to-fast light conversion in a Laguerre-Gaussian rovibrational cavity. *J. Light. Technol.* **2023**, *41*, 2246–2251. [CrossRef]
20. Cheng, H.J.; Zhou, S.J.; Peng, J.X.; Kundu, A.; Li, H.X.; Jin, L.; Feng, X.L. Tripartite entanglement in a Laguerre–Gaussian rotational-cavity system with an yttrium iron garnet sphere. *JOSA B* **2021**, *38*, 285–293. [CrossRef]
21. Wang, F.; Shen, K.; Xu, J. Rotational mirror-mirror entanglement via dissipative atomic reservoir in a double-Laguerre-Gaussian-cavity system. *New J. Phys.* **2023**, *24*, 123044. [CrossRef]
22. Walls, D.; Milburn, G. *Quantum Optics*; Springer Science & Business Media: Berlin/Heidelberg, Germany, 2012.
23. Huang, S.; Agarwal, G. Enhancement of cavity cooling of a micromechanical mirror using parametric interactions. *Phys. Rev. A* **2009**, *79*, 013821. [CrossRef]
24. Huang, S.; Agarwal, G. Normal-mode splitting in a coupled system of a nanomechanical oscillator and a parametric amplifier cavity. *Phys. Rev. A* **2009**, *80*, 033807. [CrossRef]
25. Lü, X.Y.; Wu, Y.; Johansson, J.; Jing, H.; Zhang, J.; Nori, F. Squeezed optomechanics with phase-matched amplification and dissipation. *Phys. Rev. Lett.* **2015**, *114*, 093602. [CrossRef] [PubMed]
26. Yang, R.G.; Li, N.; Zhang, J.; Li, J.; Zhang, T.C. Enhanced entanglement of two optical modes in optomechanical systems via an optical parametric amplifier. *J. Phys. At. Mol. Opt. Phys.* **2017**, *50*, 085502. [CrossRef]

27. Mi, X.; Bai, J.; Song, K.H. Robust entanglement between a movable mirror and a cavity field system with an optical parametric amplifier. *Eur. Phys. J. D* **2013**, *67*, 115. [CrossRef]
28. Hu, C.S.; Liu, Z.Q.; Liu, Y.; Shen, L.T.; Wu, H.; Zheng, S.B. Entanglement beating in a cavity optomechanical system under two-field driving. *Phys. Rev. A* **2020**, *101*, 033810. [CrossRef]
29. Hu, C.S.; Huang, X.R.; Shen, L.T.; Yang, Z.B.; Wu, H.Z. Enhancement of entanglement in distant micromechanical mirrors using parametric interactions. *Eur. Phys. J. D* **2017**, *71*, 1–8. [CrossRef]
30. Guo, J.L.; Zhai, L.L. Improving Atom–Mirror Entanglement and Mechanical Squeezing in a Modulated Optomechanical System. *Ann. Phys.* **2022**, *534*, 2100445. [CrossRef]
31. Giovannetti, V.; Vitali, D. Phase-noise measurement in a cavity with a movable mirror undergoing quantum Brownian motion. *Phys. Rev. A* **2001**, *63*, 023812. [CrossRef]
32. Gardiner, C.; Zoller, P. *Quantum Noise: A Handbook of Markovian and Non-Markovian Quantum Stochastic Methods with Applications to Quantum Optics*; Springer Science & Business Media: Berlin/Heidelberg, Germany, 2004.
33. DeJesus, E.X.; Kaufman, C. Routh-Hurwitz criterion in the examination of eigenvalues of a system of nonlinear ordinary differential equations. *Phys. Rev. A* **1987**, *35*, 5288. [CrossRef] [PubMed]
34. Benguria, R.; Kac, M. Quantum langevin equation. *Phys. Rev. Lett.* **1981**, *46*, 1. [CrossRef]
35. Adesso, G.; Serafini, A.; Illuminati, F. Extremal entanglement and mixedness in continuous variable systems. *Phys. Rev. A* **2004**, *70*, 022318. [CrossRef]
36. Vidal, G.; Werner, R.F. Computable measure of entanglement. *Phys. Rev. A* **2002**, *65*, 032314. [CrossRef]
37. Gigan, S.; Böhm, H.; Paternostro, M.; Blaser, F.; Langer, G.; Hertzberg, J.; Schwab, K.C.; Bäuerle, D.; Aspelmeyer, M.; Zeilinger, A. Self-cooling of a micromirror by radiation pressure. *Nature* **2006**, *444*, 67–70. [CrossRef] [PubMed]
38. Simon, R.; Sudarshan, E.; Mukunda, N. Gaussian-Wigner distributions in quantum mechanics and optics. *Phys. Rev. A* **1987**, *36*, 3868. [CrossRef]
39. Asjad, M.; Tombesi, P.; Vitali, D. Feedback control of two-mode output entanglement and steering in cavity optomechanics. *Phys. Rev. A* **2016**, *94*, 052312. [CrossRef]
40. Li, J.; Li, G.; Zippilli, S.; Vitali, D.; Zhang, T. Enhanced entanglement of two different mechanical resonators via coherent feedback. *Phys. Rev. A* **2017**, *95*, 043819. [CrossRef]